Program Digest, 2019 IEEE International Ultrasonics Symposium (IUS)
Glasgow, Scotland, October 6-9, 2019

Large Field-Of-View Shear Wave Elasticity Imaging with Combined On- and Off-Axis Stiffness Estimation for High Frame Rate Hepatic HCC Screening

Courtney A. Trutna, Samantha L. Lipman, Mark L. Palmeri, and Kathryn R. Nightingale
Department of Biomedical Engineering, Duke University, Durham, NC, USA
email: courtney.trutna@duke.edu

***Abstract*—Heptaocellular carcinoma (HCC) is a commonly occurring cancer and is currently detected using B-mode ultrasound scans in at-risk patients. However, B-mode ultrasound has low sensitivity for HCC, particularly for early stage disease. Ultrasound elasticity imaging methods have been used to demonstrate a stiffness contrast between HCC lesions and the surrounding liver, but currently, these elasticity methods are limited to small fields of view (3x3 cm^2), such that full liver elasticity screenings would be excessively time consuming. Previous work has simulated a large field-of-view shear wave elasticity imaging sequence with on-axis reconstruction techniques. This work demonstrates this sequence and reconstruction strategy in phantoms, including an experimentally developed lookup table for the on-axis reconstruction. Results are presented for both a homogeneous and lesion-containing phantom. In the homogeneous phantom, the experimentally derived lookuptable exhibits less bias in the on-axis reconstruction than when using a simulation-based lookup table. In the lesion phantom, three lesions are measured and found to have similar shear wave speed values and contrasts to the manufacturer quoted values. Overall, a field of view of 68 cm^2 is obtained using 3 overlapping SWEI reconstruction regions.**

I. Introduction

Hepatocellular carcinoma (HCC) is the sixth most diagnosed cancer and fourth leading cause of cancer death worldwide [1]. The current standard for detecting HCC is a B-mode liver scan in at-risk patients every 6 months, followed by multiphasic MRI or multiphasic CT of any suspicious lesions identified [2], [3]. Unfortunately, B-mode screenings have a low sensitivity for HCC settings, with sensitivities as low as 58% in real world settings, and 32% for early stage disease [4].

Shear wave elasticity imaging (SWEI) has the potential to serve as an alternative screening modality. Many groups have demonstrated stiffness contrast between HCC and the surrounding liver that suggests HCC lesions may be better visualized in SWEI than in B-mode ultrasound [5]–[10]. However, current commercial implementations of SWEI only image an approximate 3 cm x 3 cm region, while B-mode imaging is capable of a field of view (FOV) near 15 cm x 15 cm. Because of this small FOV, SWEI screening of the liver would be excessively time consuming for both the patient and healthcare provider.

Previous work from our group has simulated a technique for large FOV 2D SWEI [11]. This technique uses multiple sequential angled ARFI pushes to create a large region of shear wave speed (SWS) reconstruction. Additionally, a the on-axis region of each push is reconstructed using a time-to-peak (TTP) displacement lookup table. This lookup table is a function of the specific probe geometry, angle of push, and the point of observation (axial depth and distance from the center line of the push). This on-axis lookup table allows for an extended continuous FOV to be captured with fewer ARFI excitations, as it removes the need for a SWS reconstruction region to overlap the on-axis region of the neighboring reconstruction for a continuous SWS image.

Herein, we present an experimental implementation of the large FOV 2D SWEI sequence and on-axis reconstruction method. Notably, these experiments are subject to the effects of ultrasonic displacement tracking, which had not been modeled in the previous simulation work. To adjust for the effects of tracking in the on-axis reconstruction, a lookup table was created through experimental acquisitions in a number of calibrated elasticity phantoms.

II. Methods

A. Experimental Sequence

All measurements were performed using a C52 transducer using a Vantage 256 Verasonics research scanner (Verasonics, Redmond, WA, USA). The full FOV was interrogated using three separate SWEI sequences, performed sequentially, which were combined after performing all SWS reconstruction. These three sequences used ARFI push angles of -20, 0 and 20 degrees. Each ARFI push was generated using a supersonic, multifocal push with foci at 7.5, 5.5 and 4 cm in depth [12]. Each sub-push consisted of 200 cycles at a frequency of 2.3 MHz, and the F-number was held constant at 2.3. The resultant shear wave was tracked using plane wave tracking with a pulse repetition frequency (PRF) of of 5 kHz. Displacement estimation was performed using the Kasai algorithm [13].

Each SWEI sequence was used to reconstruct the SWS for ±25 mm perpendicular to the ARFI push. These regions were reconstructed in two parts. The "off-axis" region, considered to be >3 mm away from the center line of the ARFI excitation, was estimated using 3D directional filtering and 2D (lateral and axial) normalized cross correlation, as in [11]. The "on-axis" region was estimated using the lookup table technique described below. The results from the 3 SWEI sequences were combined, with averaging performed for any overlapping reconstruction areas. A 5x5 pixel median filter was applied to the final reconstructed SWS maps, and values greater than 12 m/s were removed.

B. On-Axis Reconstruction

The on-axis lookup table was created using a series of experimental acquisitions in calibrated elasticity phantoms. Acquisitions were performed in six phantoms (3, 5.8, 12, 18.5, 35.5 and 69.7 kPa), with the sequence and displacement tracking as described above. These acquisitions were processed using the following procedure. First, the first time step after the ARFI push was removed due to reverberation, leaving the first time step recorded at 0.8 ms for this sequence. The data was then low pass filtered (third order, zero-phase Butterworth filter with a cutoff frequency of 1 kHz). The TTP displacement was then calculated for all positions within the on-axis range. Three-point quadratic peak interpolation was used to allow the TTP displacement to take on values other than those determined by the PRF of the ultrasonic tracking. A 1 mm smoothing filter was applied to the TTP displacement data to smooth the jitter from the ultrasonic tracking, and TTP displacement values greater than 10 ms were discarded. Ten independent speckle realizations were averaged for the zero degree push. For the angled pushes, the lookup table is assumed to be symmetric for push angles of the same absolute value. The 20 degree lookup table was created by averaging 5 independent speckle realizations each from pushing at -20 degrees and 20 degrees. This TTP displacement data were then smoothed axially using a 7.5 mm kernel. Three example TTP displacement curves through depth are shown in Fig. 1 for two distances from the centerline (solid r=0 mm, dashed r=2 mm), both for the zero-degree push angle. Finally, the lookup table is compiled by interpolating between these reference TTP displacements in known materials to estimate the material properties for a given arbitrary TTP displacement. The final lookup table is a function of the radial depth, distance from the push centerline, and the absolute value of the push angle.

Experimental acquisitions were processed using the same steps as described above. The TTP displacement values from an experimental acquisition were then used in conjunction with the lookup table to arrive at a stiffness estimate for the on-axis region. Note that the reference phantom values are reported in Young's modulus [kPa]; however, the reconstructions are given in SWS [m/s]. In this work, we have assumed an elastic, incompressible material, and thus the conversion between these values is $SWS = \sqrt{\frac{E}{3\rho}}$, where E is the Young's

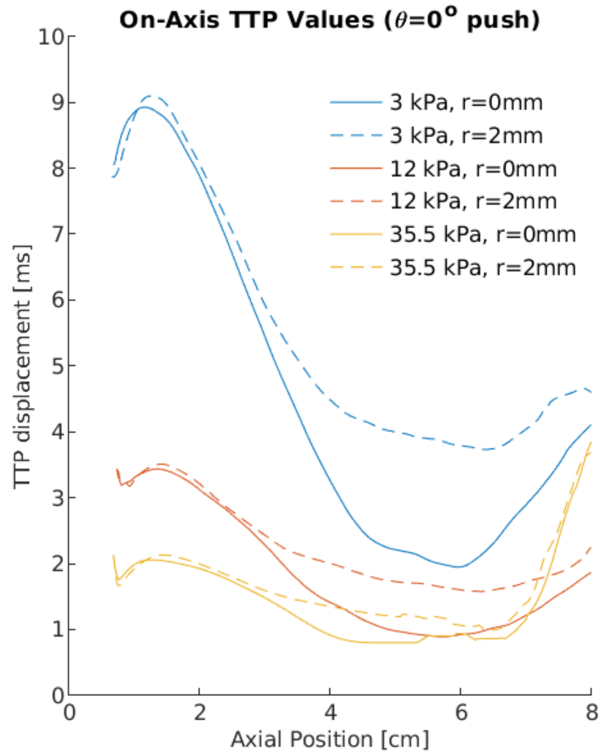

Fig. 1. Averaged experimental TTP displacement curves in 3 elastic phantoms (3, 12 and 35.5 kPa). Curves were created through the process described in Section II.B. All curves show results for the zero degree push, with the solid lines showing the results along the push centerline (r=0mm) and dashed lines showing the results 2mm away from the push centerline (r=2mm). In general, the TTP displacement is greater in softer materials, and is greater for positions away from the push centerline.

modulus and ρ is the density of the material, assumed to be 1000 kg/m^3.

III. Results

Fig. 2 shows the results from a large FOV SWEI sequence and reconstruction in a homogeneous, 12 kPa (2 m/s) phantom. Due to the lateral size of the phantom (10 cm laterally), the FOV visualized is actually smaller than the FOV that is possible with this sequence. We note that the SWS reconstruction is homogeneous across the FOV, as expected. There are remaining jitter artifacts in the on-axis reconstruction, however, they do not impede the ability of the observer to determine that no lesion is present. The overall reconstructed SWS has a mean value of 2.20 m/s and a median value of 2.02 m/s.

Fig. 3 shows a histogram of values from the on-axis reconstruction using the newly-developed, experimental lookup table and the same histogram when using a simulated lookup table. This simulated lookup table was developed following the techniques of [11], but for the specific probe geometry used herein, which differs from that work. When using the simulated lookup table, a substantial bias in the on-axis reconstruction is observed relative to the true value of 2 m/s, with a

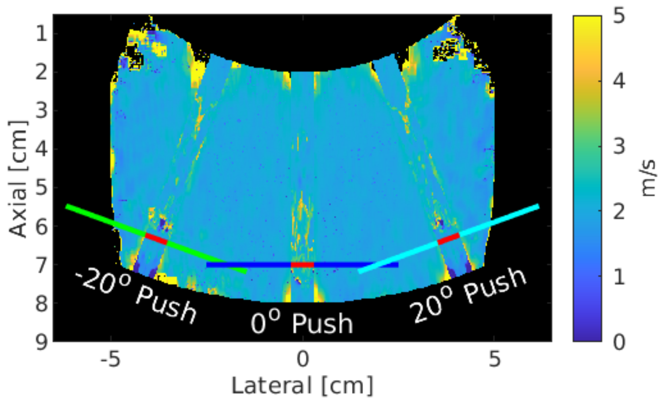

Fig. 2. Large FOV SWEI acquisition in a homogeneous, 12kPa (2 m/s) phantom. The SWS across the reconstructed map has a mean value of 2.20 m/s and a median value of 2.02 m/s. Black regions represent areas that were outside of the phantom, outside of the FOV, or where the reconstructed value was excluded (>12 m/s). The three reconstruction regions are labeled in green, blue and cyan across the bottom of the image. The region of on-axis reconstruction is highlighted in red within these labels.

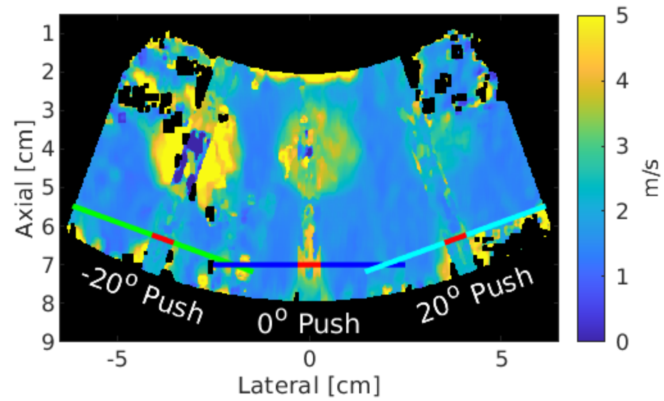

Fig. 4. Large FOV SWEI acquisition in a lesion-containing phantom. Three lesions are visible, the measurements of which are presented in I. The background value across the FOV was measured as 2.0 ± 1.0. Black regions represent areas outside the FOV or where the reconstructed value was excluded (>12 m/s). The three reconstruction regions are labeled in green, blue and cyan across the bottom of the image. The region of on-axis reconstruction is highlighted in red within these labels.

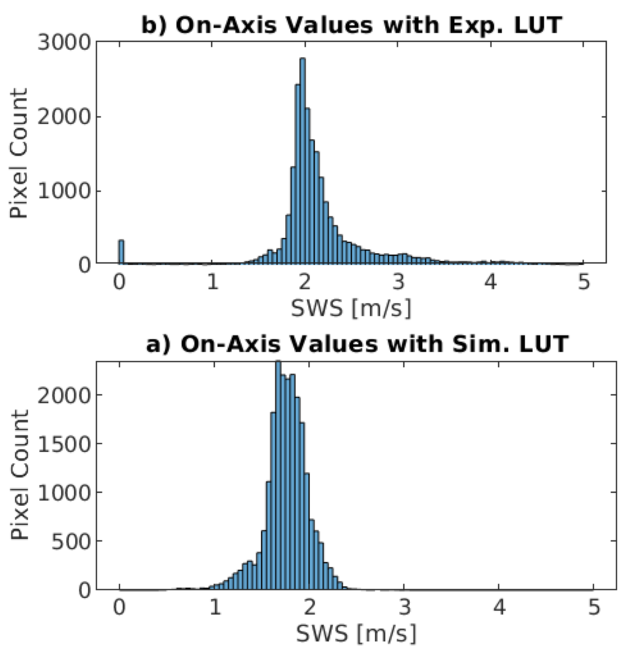

Fig. 3. Histograms of the reconstructed on-axis values in a homogenous 12 kPa (2 m/s) phantom. A) Reconstruction using the experimental (phantom acquisition) based LUT. B) Reconstruction using the simulation based lookup table (LUT). The simulation LUT exhibits a bias relative to the true value (mean 1.76 m/s, median 1.77 m/s), while the experimental LUT reduces this bias (mean 2.16, median 2.05 m/s). Noise from the ultrasonic tracking (jitter) is visible in the experimental LUT reconstruction.

mean value of 1.76 m/s and a median value of 1.77 m/s. When using the experimental lookup table, the on-axis reconstruction is less biased, with a mean value of 2.16 m/s and a median value of 2.05 m/s.

Fig. 4 shows the results from a large FOV SWEI sequence and reconstruction in a phantom with lesions. Three lesions are visible in this view. The background value was estimated at 2.0 ± 1.0 m/s. The experimental values, contrast and CNR along with the manufacturer quoted values and contrast are shown in Table I. Overall, the values and contrast measurements agree. In this SWS image, a FOV of 68 cm^2 was acquired.

TABLE I
LESION MEASUREMENTS

Lesion	Left	Center	Right
SWS ± Std. Dev. [m/s]	3.9 ± 2.0	3.3 ± 0.7	2.5 ± 0.5
Contrast	0.94	0.64	0.20
CNR	0.87	1.10	0.39
Quoted value [m/s]	4.40	2.91	2.33
Quoted contrast	1.41	0.59	0.28

IV. DISCUSSION

We have demonstrated large FOV SWEI imaging experimentally in phantoms. The on-axis reconstruction method allows for fewer ARFI pushes to be used to interrogate a large FOV while still forming a continuous SWS image. In this sequence, each of the 3 SWEI reconstruction regions was imaged in approximately 21 ms, leading to a full imaging time of 63 ms. This corresponds to a hypothetical SWEI frame rate of >15 fps for the entire FOV. However, because of the time taken to transfer data and perform the computationally-intensive cross correlations used for the SWS estimation, all processing was done offline. Future hardware and software development would be needed to enable real-time processing and display.

The experimental based lookup table is necessary to account for the effects of ultrasonic displacement tracking. When using a lookup table developed from simulated materials for the lookup table (without tracking), the on-axis reconstruction is biased low relative to the true values. Fig 3. demonstrates that the first-order effects of tracking are accounted for when using the experimental lookup table. However, the effects of the abdominal body wall when scanning *in vivo*, particularly aberration that distorts the tracking beam profile, may change the TTP displacement values for a given material, leading to an error in the on-axis reconstruction. The degree of this effect is the subject of future investigations.

Additionally, the TTP displacement on-axis lookup table encounters challenges in stiffer materials. Near the focal region, stiff materials can have TTP displacement values near or before the first imaging timestep. This is visible in Fig. 1, where the 35.5 kPa phantom at r=0 mm (solid yellow line) is measured to have a TTP displacement of 0.8 ms near the focal region, equivalent to the first recorded tracking time step. An earlier TTP displacement cannot be detected, and so bias may be present in the TTP displacement of the 35.5 kPa phantom, and a stiffer material could not be accurately characterized in this region by this technique. However, this concern is mitigated with increased distance between the observation point and the focal zone, both laterally and axially. As Fig. 1 shows, at a lateral distance of 2 mm from the center focal line, the TTP displacements are captured even for stiff materials. Additionally, while the limitations of TTP displacement may bias the on-axis estimates of stiff materials, the overall goal of this work is to enable the identification of suspicious lesions in the context of HCC screening. An accurate estimate of the stiffness of these lesions is not necessary to identify suspicious regions for follow up imaging with other modalities. Thus, this limitation within stiff (and thus already suspicious) materials is not of first-order concern for this work. Nonetheless, future work will explore other measurements to employ in the on-axis lookup table to reduce the jitter noise and provide more robust estimates in stiff materials.

A major factor in the FOV reconstructed is the range over which a shear wave travels. This experimental demonstration in phantoms assumes a lateral SWS propagation region of 25 mm. A smaller lateral reconstruction range would likely be necessary for reliable reconstruction *in vivo* due to the effects of the body wall and shear attenuation of the liver. This could be corrected with more pushes at more angles (for example -20, -10, 0, 10, and 20^o, as was used in [11]), but would decrease the overall framerate of the sequence.

Finally, work is ongoing in our lab to extend this large FOV 2D SWEI sequence to 3D imaging, which will additionally track shear wave propagation in the elevational dimension. This will interrogate a volume of tissue with each acquisition, rather than a 2D slice, thus further reducing the time to screen the entire organ for lesions.

V. Conclusion

A large FOV SWEI sequence is demonstrated in phantoms, including a method for on-axis reconstruction using an experimentally developed lookup table. This expanded FOV could enable elasticity screenings for HCC lesions in a scan time comparable to current B-mode screenings. Future work will explore in vivo demonstration of the on-axis technique and large FOV sequence, as well as alternative on-axis measurements and 3D SWEI imaging.

Acknowledgment

The authors would like to thank Ned Danieley for computer system administration and NIH funding sources R01-EB022106 and T32-EB001040.

References

[1] F. Bray, J. Ferlay, I. Soerjomataram, R. L. Siegel, L. A. Torre, and A. Jemal, "Global cancer statistics 2018: GLOBOCAN estimates of incidence and mortality worldwide for 36 cancers in 185 countries." *CA: a cancer journal for clinicians*, vol. 68, no. 6, pp. 394–424, 2018. [Online]. Available: http://www.ncbi.nlm.nih.gov/pubmed/30207593

[2] P. R. Galle, A. Forner, J. M. Llovet, V. Mazzaferro, F. Piscaglia, J. L. Raoul, P. Schirmacher, and V. Vilgrain, "EASL Clinical Practice Guidelines: Management of hepatocellular carcinoma," *Journal of Hepatology*, vol. 69, no. 1, pp. 182–236, 2018. [Online]. Available: http://dx.doi.org/10.1016/j.jhep.2011.12.001

[3] L. M. Kulik, M. H. Murad, R. S. Finn, J. A. Marrero, J. K. Heimbach, A. X. Zhu, C. B. Sirlin, M. M. Abecassis, and L. R. Roberts, "AASLD guidelines for the treatment of hepatocellular carcinoma," *Hepatology*, vol. 67, no. 1, pp. 358–380, 2018.

[4] A. G. Singal, H. S. Conjeevaram, M. L. Volk, S. Fu, R. J. Fontana, F. Askari, G. L. Su, A. S. Lok, and J. A. Marrero, "Effectiveness of hepatocellular carcinoma surveillance in patients with cirrhosis," *Cancer Epidemiology Biomarkers and Prevention*, vol. 21, no. 5, pp. 793–799, 2012. [Online]. Available: www.aacrjournals.org

[5] A. Guibal, C. Boularan, M. Bruce, M. Vallin, F. Pilleul, T. Walter, J. Y. Scoazec, N. Boublay, J. Dumortier, and T. Lefort, "Evaluation of shearwave elastography for the characterisation of focal liver lesions on ultrasound," *European Radiology*, vol. 23, no. 4, pp. 1138–1149, 2013.

[6] H. S. Park, Y. J. Kim, M. H. Yu, S. I. Jung, and H. J. Jeon, "Shear wave elastography of focal liver lesion: Intraobserver reproducibility and elasticity characterization," *Ultrasound Quarterly*, vol. 31, no. 4, pp. 262–271, 2015.

[7] Q. Lu, W. Ling, C. Lu, J. Li, L. Ma, J. Quan, D. He, J. Liu, J. Yang, T. Wen, H. Wu, H. Zh, and Y. Luo, "Hepatocellular Carcinoma: Stiffness Value and Ratio to Discriminate Malignant from Benign Focal Liver Lesions," *Radiology*, vol. 275, 2015. [Online]. Available: www.rsna.org/rsnarights.

[8] L. Gerber, D. Fitting, K. Srikantharajah, N. Weiler, G. Kyriakidou, J. Bojunga, F. Schulze, D. Bon, S. Zeuzem, and M. Friedrich-Rust, "Evaluation of 2D-Shear Wave Elastography for Characterisation of Focal Liver Lesions," *J Gastrointestin Liver Dis*, vol. 26, pp. 283–290, 2017. [Online]. Available: http://dx.doi.org/10.15403/jgld.2014.1121.263.dsh

[9] K. L. Choong, Y. H. Wong, C. H. Yeong, G. K. Gnanasuntharam, K. L. Goh, B. K. Yoong, N. Pongnapang, and B. J. J. Abdullah, "Elasticity Characterization of Liver Cancers Using Shear Wave Ultrasound Elastography: Comparison Between Hepatocellular Carcinoma and Liver Metastasis," *Journal of Diagnostic Medical Sonography*, vol. 33, no. 6, pp. 481–488, 2017.

[10] H. Nagolu, S. Kattoju, C. Natesan, M. Krishnakumar, and S. Kumar, "Role of Acoustic Radiation Force Impulse Elastography in the Characterization of Focal Solid Hepatic Lesions," *2*, vol. 8, no. 1, p. 5, 2018. [Online]. Available: http://www.ncbi.nlm.nih.gov/pubmed/29541491 http://www.pubmedcentral.nih.gov/articlerender.fcgi?artid=PMC5843967

[11] S. L. Lipman, M. L. Palmeri, and K. R. Nightingale, "Large Field-of-View Shear Wave Imaging for Hepatocellular Carcinoma Screening," in *Proceedings of the IEEE Interational Ultrasonics Symposium*. IEEE, 2018, pp. 1–4.

[12] J. Bercoff, M. Tanter, and M. Fink, "Supersonic shear imaging: A new technique for soft tissue elasticity mapping," *IEEE Transactions on Ultrasonics, Ferroelectrics, and Frequency Control*, vol. 51, no. 4, pp. 396–409, 2004.

[13] C. Kasai, K. Namekawa, A. Koyano, and R. Omoto, "Real-Time Two-Dimensional Blood Flow Imaging Using an Autocorrelation Technique," *IEEE Trans. Sonics Ultrason.*, vol. 32, no. 3, 1985.